View metadata, citation and similar papers at core.ac.uk

brought to you by CORE

provided by Elsevier - Publisher Connector

Sensing and Bio-Sensing Research 11 (2016) 37–44

Contents lists available at ScienceDirect

Sensing and Bio-Sensing Research

journal homepage: www.elsevier.com/locate/sbsr

Gold nanoparticles encapsulated in a soda-lime glass substrate for plasmonic temperature sensing

Jacqueline Elwood [a], Zhouying Zhao [a], Lawrence M. Saupe [b], T. Darton Strayer [b], Randall N. Odell [b], Michael A. Carpenter [a,*]

[a] College of Nanoscale Science and Engineering, SUNY Polytechnic Institute, Albany, NY, United States
[b] Bechtel Marine Propulsion Corporation, Niskayuna, NY, United States

ARTICLE INFO

Article history:
Received 14 March 2016
Received in revised form 7 October 2016
Accepted 11 October 2016

Keywords:
Localized surface plasmon resonance
Au nanoparticle
Pure temperature sensing
Fully encapsulation

ABSTRACT

We present a study on the temperature response of the plasmon peak of gold nanoparticles (AuNPs) completely encapsulated in soda-lime glass for temperatures ranging from 298 K to 723 K and in ambient pressure air, Ar and aqueous environments. The observed peak position changed with temperature in a linear manner, as expected from the theoretical model also presented in this study. The linear character was upheld in different gaseous environments of inert Ar and ambient air, as well as in both pure deionized water and acidic water. The consistent expected dependence provided proof of the versatility of the encapsulated AuNPs and their robustness to be able to withstand both high temperature and high acidity and still retain their sensing capability.

© 2016 The Authors. Published by Elsevier B.V. This is an open access article under the CC BY-NC-ND license (http://creativecommons.org/licenses/by-nc-nd/4.0/).

1. Introduction

Sensors that rely on the principle of localized surface plasmon resonance (LSPR) of metal nanoparticles (NPs) have gained popularity in chemical and biological applications due to its tenability, label-free sensing, and sensitivity [1–5]. Extensive studies on the ability for LSPR-based sensors to operate at high temperatures have already been established [6], but no pure temperature sensor has been developed. The temperature effect of noble metal NPs has been studied [6,7], but these studies are normally done with NPs embedded in porous silica matrix, which will not be able to isolate a chemical effect in ambient environments.

The plasmonic properties of AuNPs are sensitive to changes in temperature due to three effects: 1) electron-phonon scattering in the NP, 2) thermal expansion of the NP, and 3) temperature dependence of the dielectric permittivity of the host matrix [6,7]. From the Drude model (Eq. (1)), the peak frequency of the plasmon peak position, Ω, is shown to be strongly influenced by the free electron density of the NPs (N / R [3]), where N is the number of free electrons and R is the radius of the NPs. Ω is also influenced by e, the elementary charge, ε_m the dielectric function of the matrix surrounding the NPs, χ^{ib1} (the real part) the interband transition dependence of the dielectric function of the NPs, γ the damping constant, m_e the electron mass and ε_o the vacuum permittivity [8].

$$\Omega = \sqrt{\frac{Ne^2}{(1+2\varepsilon_m+\chi^{ib1})m_e 4\pi\varepsilon_o R^3} - \gamma^2} \quad (1)$$

The damping constant is given by

$$\gamma = \gamma_\infty(T) + A\frac{V_F}{R} \quad (2)$$

where γ_∞ is the size-independent damping constant resulting from the scattering of electron with electron, phonon, and lattice defects, A is a theory-dependent parameter detailing the scattering process, and V_F is the Fermi velocity in bulk metal (1.29×10^8 cm/s for gold). For changes in the peak position of the plasmon resonance, a change in the size of the NP due to thermal expansion will reduce the free electron density of the NP, thus, causing a red shift in the plasmon band towards longer wavelengths. Electron-phonon scattering and changes in the dielectric permittivity are also affected by an increase in temperature but cause only minor shifts towards redder wavelengths of the plasmon band. The full width at half maximum (FWHM) of the plasmon band is also affected by an increase in temperature and generally broadens as a result, with electron-phonon scattering being the dominant contribution in the increasing FWHM with temperature. This theory was proven to

* Corresponding author.
E-mail address: mcarpenter@sunypoly.edu (M.A. Carpenter).

http://dx.doi.org/10.1016/j.sbsr.2016.10.003
2214-1804/© 2016 The Authors. Published by Elsevier B.V. This is an open access article under the CC BY-NC-ND license (http://creativecommons.org/licenses/by-nc-nd/4.0/).

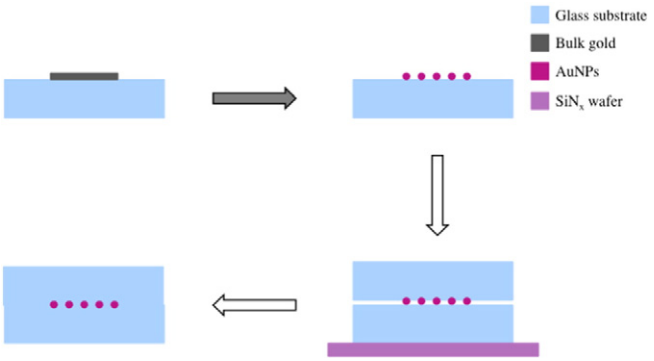

Fig. 1. Fabrication process for the embedded sample.

hold under experimental testing with AuNPs of various sizes in a silica matrix [7].

Theoretically, both temperature and chemical effects influence the LSPR properties of AuNPs. Composition of the surrounding environment will cause shifts in the peak position of the Au plasmon peak, a principle that has been traditionally used for plasmonic chemical sensing at high-temperatures [6,9]. By eliminating this chemical effect, a pure temperature measurement can be created that relies on this popular LSPR-based sensing mechanism. Isolation of the AuNPs from ambient environments by fully embedding the particles in a glass matrix can prevent chemical effects on the NPs, allowing for the development of a pure temperature sensor that can be used in different environments [6].

2. Experimental

Two samples of AuNPs embedded in glass were prepared to study the temperature dependence of the LSPR of Au. One sample was a shallow-embedded sample of AuNPs in a 1-mm thick piece of soda-lime-silica glass and the other sample was a deep-embedded sample of AuNPs sandwiched between two pieces of the same type of glass. A 5 nm-thick Au thin film was thermally evaporated onto the glass and then annealed at 400 °C for 10 min to form the AuNPs on the surface. To create either the shallow-embedded or the deep-embedded AuNPs, the sample was further annealed at a higher temperature without or with being placed with another piece of 1-mm thick soda-lime glass. The pieces were annealed on a SiN_x coated silicon wafer at 660 °C, well above the glass transition temperature of 540 °C for soda-lime glass, for 6 h in static air. This allowed the AuNPs to sink into the glass or made the pieces of glass fuse together, trapping or sealing the AuNPs inside as shown in Fig. 1 for the deep-embedded AuNPs sample. The sample was then cooled at a rate of 1 °C/min to 400 °C, 1.5 °C/min to 200 °C, and, finally, natural cooling to 25 °C.

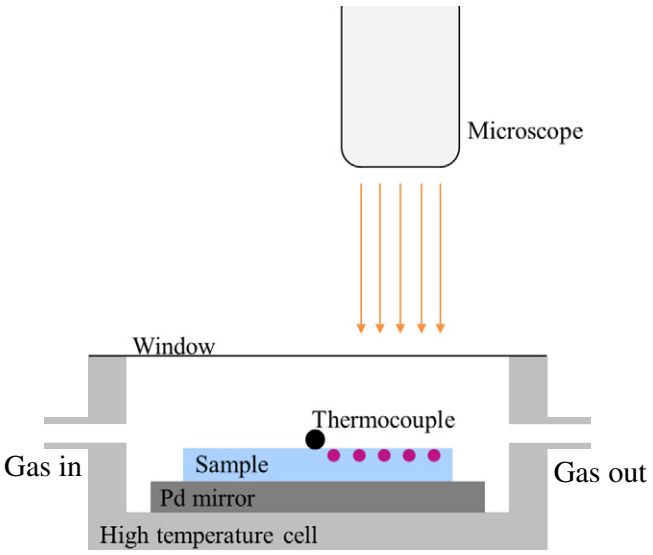

Fig. 3. Schematic diagram of set up for reflection tests.

The embedded glass samples were first used to investigate the AuNP's temperature dependence in transmission mode. The sample was mounted on a Macor holder and placed into a quartz flow tube as shown in Fig. 2. In this setup two detectors are used to monitor sensing signal and light source stability for real time correction, respectively. Tests were done by exposing the sample to both air and Ar at different temperatures ranging from room temperature to 450 °C (far below the glass transition point), taking a spectrum of the NPs every 10 s. At the highest temperature, the gas flow was switched to 1% H_2 in air to test for chemical inertness.

For reflectance mode measurements, the deep-embedded sample was too thick to achieve focus in the small high temperature cell so the shallow-embedded sample had to be used. The sample was placed onto a Pd mirror in the high temperature cell as seen in Fig. 3. A thermocouple was directly mounted on the sample surface to ensure accurate temperature reading near the AuNPs for better curve fitting. Reflected light was collected by a microscope objective and then detected using an Ocean Optics UV–vis spectrometer. The sample was tested in 5% O_2 in Ar at temperatures ranging from room temperature to 350 °C for 1 h at each temperature step, like the tests in transmission mode, a spectrum of the sample was taken every 10 s.

Finally, testing of the temperature dependence of the plasmonic properties of AuNPs was done in water. For this experiment, the sample was placed between a quartz window and a reflector. The sample and reflector were suspended from a tube and allowed to be submerged in water. The window provided a barrier between water and the inside

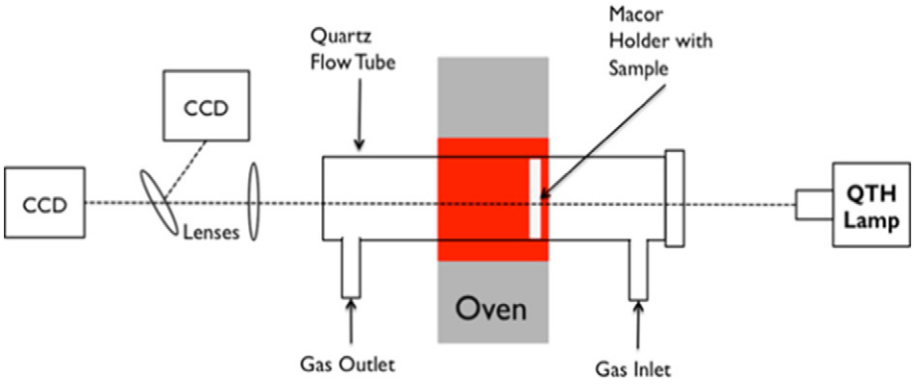

Fig. 2. Schematic diagram of set up for transmission tests.

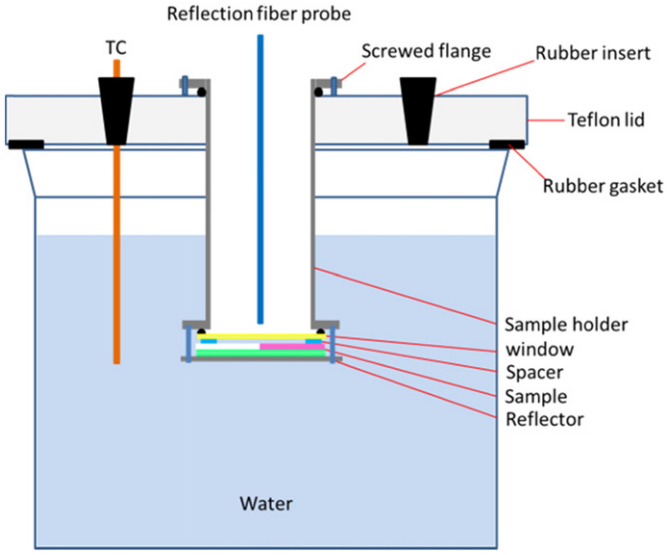

Fig. 4. Schematic diagram of set up for water tests.

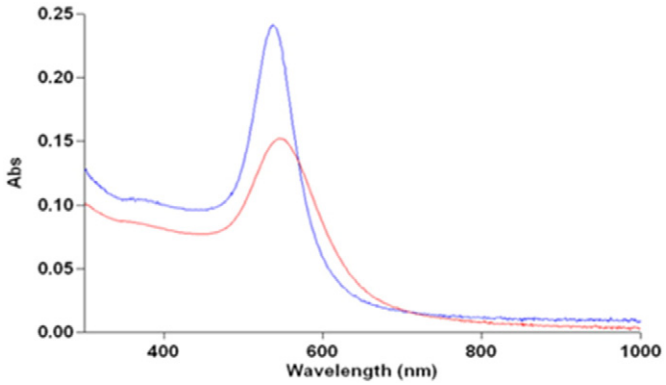

Fig. 6. LSPR spectra of embedded (blue curve) and non-embedded (red curve) AuNPs.

of the tube, which was exposed to ambient air. The optical fiber probe was lowered into this tube to do reflection measurements of the sample in water. A Teflon lid was created to hold the sample holder stable in the water and also held a thermocouple in place so that an accurate measurement of the water could be taken. The thermocouple was adjusted to be level with the sample so that the measurement by the thermocouple was more indicative of the temperature of the water at the sample. A schematic of this set up for the water tests can be seen in Fig. 4. The reflection probe was lowered above the sample and focused using a translational xyz stage to produce the strongest signal at a desired interrogation point. The spacers were used to make the sample exposed to water for thermal conduction while minimizing bubble formation. A spectrum of the embedded AuNPs submerged in water was taken every 10 s for the duration of the experiment. The temperature of the water was changed between room temperature and 99 °C in regular intervals with 1 h for stabilization at each temperature step. Heat to the water bath was added by a heating mantle setup with a controller. The water was kept just below the boiling point to deter the formation of bubbles on the window, which would cause interference in LSPR measurements. Finally, one last set of experiments was performed by changing the pH of the water bath via the addition of nitric acid. These measurements were collected in a similar manner as previous ones.

The formed AuNPs were characterized with scanning electron microscopy (SEM) and particle size analysis. For UV–vis spectroscopy analysis, a Lorentzian fit of each spectrum was done to find their peak positions. The peak positions were plotted as a function of time to demonstrate the shift in the LSPR peak position when the temperature was changed. The average peak position was found for each temperature step and plotted as a function of temperature to find the linear relationship between peak position and temperature. This was done for each experiment to find a correlation for transmission mode, reflection mode, and in water.

3. Results and discussion

An SEM image of the AuNPs on glass is shown in Fig. 5a and the size distribution of the NP diameters at room temperature is shown in Fig.5b. The thermally formed and stabled AuNPs are seen well-separated on the substrate as a monolayer, thus are less likely to agglomerate upon embedded or sealed between the two pieces of 1 mm glass plates (Fig. 1) at the glass fusing temperature of 660 °C. From Fig. 5b, it can be assumed that the mean diameter of the NPs is ~20 nm, near the peak of the fit to the histogram.

The room temperature absorbance spectrum of the AuNPs before and after embedding in the glass substrate is shown in Fig. 6. As can be seen, the plasmon peak position increased in intensity while the peak wavelength decreased. While encapsulation is expected to increase the peak intensity of the plasmon band, the blue shift is likely an indication of full encapsulation in the glass substrate. The redder plasmonic band of the non-embedded sample is due to surface chemical effects as the spectrum was taken after the sample was exposed to ambient air. Exposure to ambient air and water likely enabled the adsorption of significant quantities of O_2 and water onto the AuNPs. This will

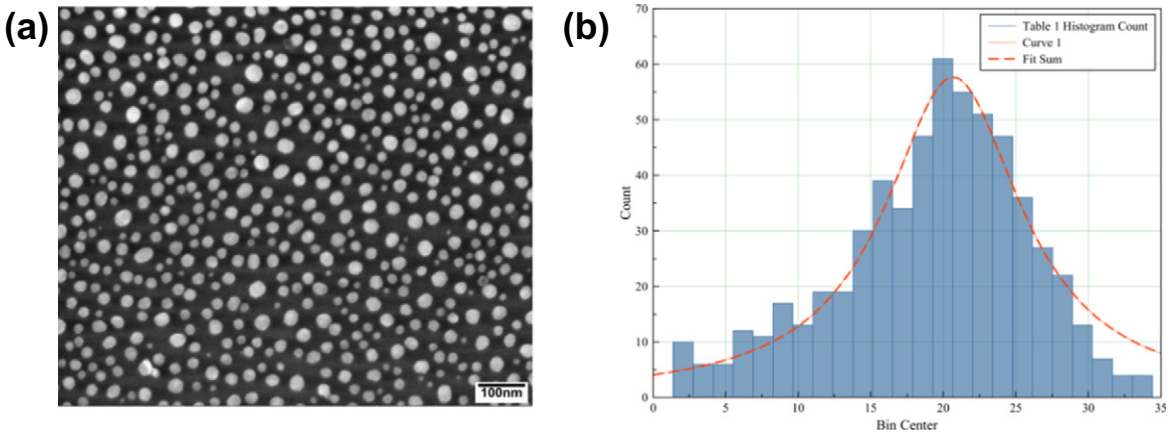

Fig. 5. (a) SEM images of AuNPs on sample and (b) accompanying size distribution of the AuNPs on the sample.

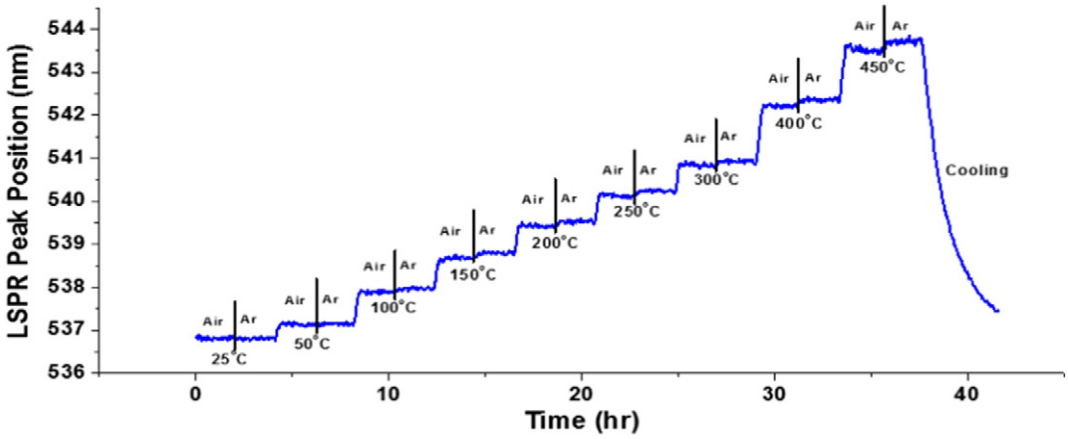

Fig. 7. LSPR peak position change with temperature with the gas changing between air and Ar.

create an effective dielectric function that is lower in value than that of the soda-lime glass. Given the relationship outlined in Eq. (1), upon desorption of the background O_2 and water and full encapsulation in the glass, there is a subsequent blue shift in the plasmon band. Importantly, the lack of red shift of plasmonic band of the AuNPs after embedding in glass confirms little or no Ostwald ripening [10] related particle agglomeration or growth at high temperature, due to the natures of the well-separated Au nanoparticle morphology (Fig. 5) and the encapsulation process.

3.1. Temperature sensing using transmission spectroscopy

Fig. 7 shows the results of the transmission mode tests, revealing a consistent red-shift of the plasmonic spectra with increasing temperature even with changing the gas chemistry. When the gas is changed between air and Ar at each temperature step, there is little change in the peak position of the LSPR band for the AuNPs while it is known that exposure to O_2 and especially to 21% of it in air can cause a noticeable red shift of the band maxima over that in Ar if the AuNPs are not embedded or sealed [11,12]. This means that the red shift in the LSPR above with temperature can be attributed completely to temperature effects and not to chemical effects for the well-sealed AuNPs. The stable LSPR band at the different elevated temperature steps including 450 °C is indeed supportive of the particle size stability due to the good sealing, which is overwhelmingly evidenced in this report. To further demonstrate the consistency in the LSPR shift with only temperature, the average peak position for each temperature and gas measurement was found and graphed as a function of temperature. As seen in Fig. 8, the nearly identical fit data of both air and Ar are linear, which would be otherwise nonlinear if there is any chemical effect superimposed. Additionally, the slopes of the air and Ar curves are similar ($0.01438 \pm 1.59 \times 10^{-4}$ nm/°C in air and $0.0146 \pm 1.87 \times 10^{-4}$ nm/°C in Ar), indicating no chemical effect on the AuNPs as the gas exposure changes. The small variation in the sensitivities at higher temperatures can be attributed to the different cooling effects associated with the gas heat transfer coefficients between Ar and air [13], with a larger cooling from air and thus slightly bluer peak positions observed at the different temperature steps.

To demonstrate that the slight LSPR peak shift in Fig. 7 is due purely to changes in cooling effects of different gases and not by any chemical effects on the AuNPs themselves, temperature calibrations were done for the sample in both air and Ar. To do this, a thermocouple was situated on the surface of the sample to measure the actual temperature at the sample surface. Then, the oven temperatures at which the sample temperature would be the same at the surface for the two different gas exposures were determined and another test was set up using this

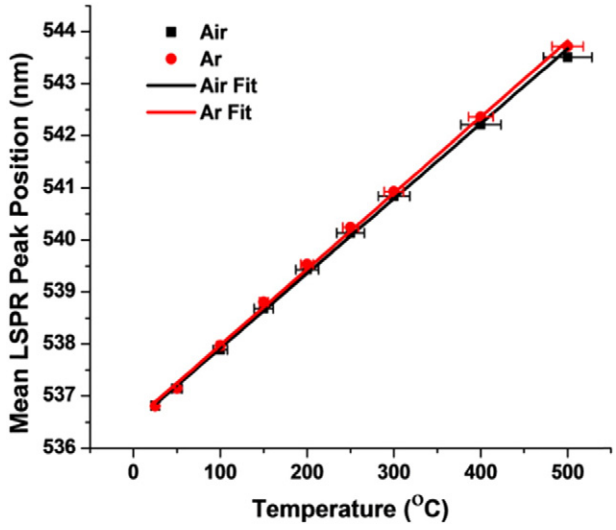

Fig. 8. Results of the transmission tests with the plot of the mean LSPR peak position as a function of temperature and the linear fit data of air and Ar.

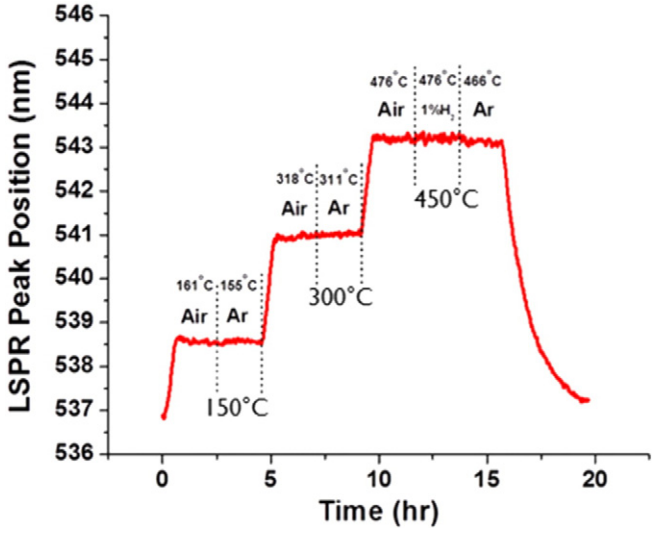

Fig. 9. Test done with temperature compensation to test for pure temperature effect on the embedded sample. The temperatures indicated on the top are the set temperatures at each gas exposure and temperature step and were determined by temperature calibration using a thermocouple placed on the backside of the sample. The lower temperature indicates the intended temperature of the sample for each temperature step.

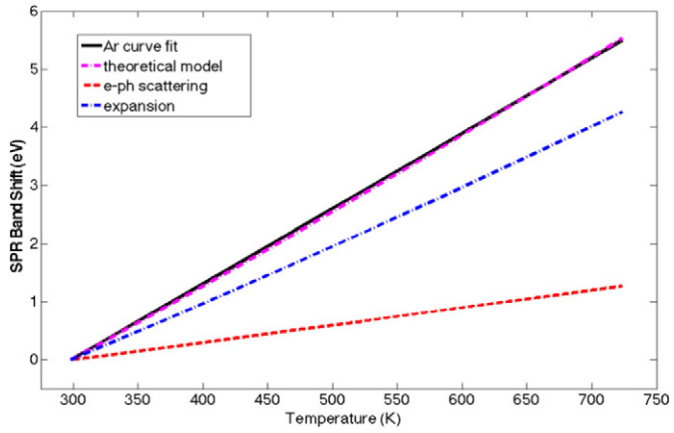

Fig. 10. Calculation of the contributions of different mechanisms to temperature induced shift of SPR in AuNPs embedded in soda-lime glass. The solid line denotes the curve fit data experimentally found for the embedded sample in Ar, the dashed line denotes the contribution from electron-phonon scattering in the NP, the blue dotted-dashed line denotes the contribution from thermal expansion of the AuNPs, and the magenta dotted-dashed line is the total shift found from the sum of the two contributions.

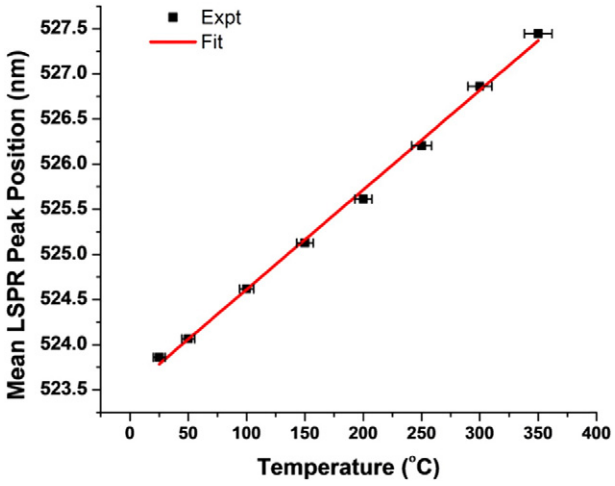

Fig. 12. Results of the reflectance tests with (a) the plot of the mean LSPR peak position as a function of temperature and (b) the linear fit data.

correction. As evidenced by Fig. 9, a consistent LSPR peak position at each sample temperature step was observed for the different gases exposed with using higher oven or set temperatures in air due to its larger cooling effect than that in Ar. At 450 °C, exposure to 1% H_2 in air does not lead to a blue shift commonly observed for non-sealed particles [11,12]. This further demonstrates the embedded AuNPs sample's sensitivity to gas cooling effects and temperature while being independent of changes in the chemical environment around the sensor.

3.1.1. Theoretical calculation of the temperature dependence of LSPR in AuNPs

The theoretical model of the various mechanisms that causes the red shift of LSPR in AuNPs with increasing temperatures follows the theory outlined by Yeshchenko et al. [7]. The temperature dependence of the LSPR of AuNPs is generally dictated by three contributions: 1) electron-phonon scattering, 2) thermal expansion of the AuNPs, and 3) the dielectric permittivity of the matrix. For the AuNPs embedded in soda-lime glass, the dielectric permittivity of the matrix changes so little in the visible wavelength region with temperature that it can be considered temperature independent [14]. This means that the change in LSPR with temperature has only two contributions.

The temperature dependence caused by electron-phonon scattering for the plasmon damping constant, $\gamma_\infty(T)$, is given by [15]

$$\gamma_\infty(T) = K\prime T^5 \int_0^{\theta/T} \frac{z^4 dz}{e^z - 1} \tag{3}$$

where θ is the Debye temperature for gold (178 K) [16] and K' is a constant. K' can be found if the damping constant, γ_∞, is known for a certain temperature, such as at $T_0 = 20$ °C, $\gamma_\infty = 0.7$ eV for gold [17]. Using these values, K' can be found via

$$K\prime = \frac{\gamma_\infty(T_0)}{T_0^5 \int_0^{\theta/T_0} \frac{z^4 dz}{e^z - 1}} \tag{4}$$

In addition to electron-phonon scattering, the change in LSPR with temperature also depends upon the thermal expansion of the AuNPs. As the temperature increases, the volume of the NPs also increases

$$V(T) = V_0(1 + \beta \Delta T) \tag{5}$$

where V_0 is the volume of the NP at room temperature calculated by finding the volume of a NP with a radius of 10 nm. $\Delta T = T - T_0$ is the absolute temperature difference between the temperature and room temperature (set at 20 °C) and β is the volume thermal expansion coefficient. Generally, the value of the volume thermal expansion coefficient can be assumed to be independent of temperature. But with the large

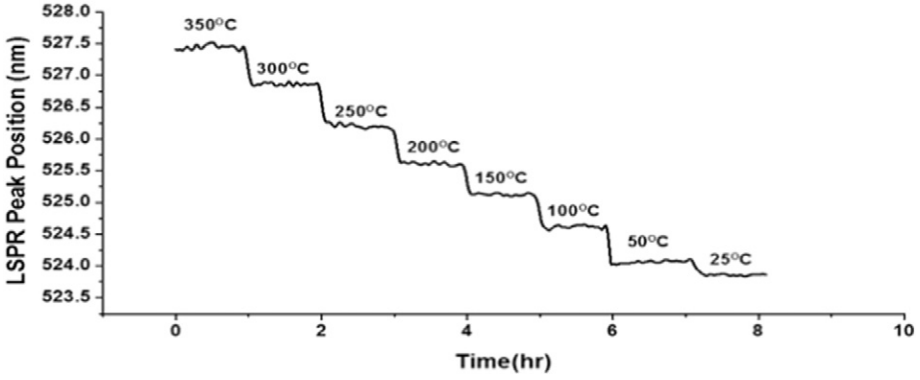

Fig. 11. Results of the reflectance tests for the shallow-embedded sample.

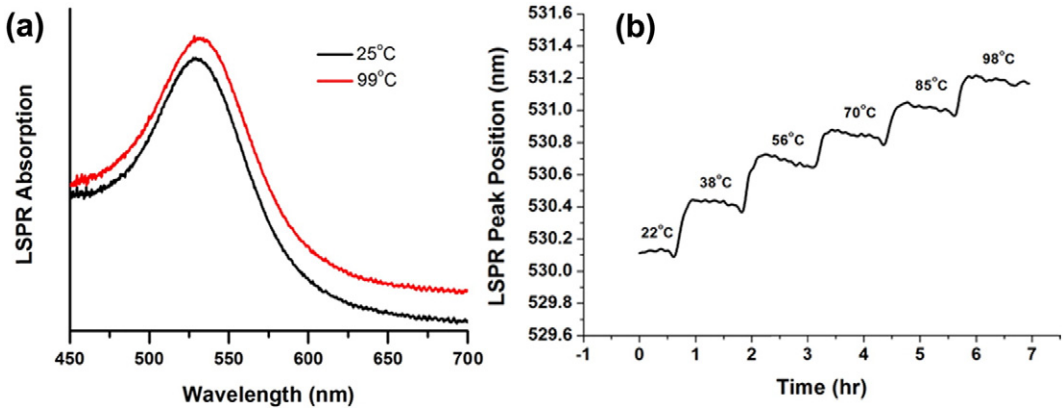

Fig. 13. (a) LSPR spectral response of AuNPs submerged in water at room temperature (black line) and 99 °C (red line) and (b) results of reflectance tests in water for the embedded sample.

range of temperatures used in this experiment, the temperature dependence of β needs to be taken into account in order to provide a more accurate model such that

$$\beta(T) = \frac{192\rho k_b}{r_0\phi(16\rho - 7Tk_b)^2} \tag{6}$$

where k_b is the Boltzmann constant, and r_0, ϕ, and ρ are parameters of the Morse potential for gold and are given by Yeshchenko et al. [7].

Eqs. (3)–(5) were used to calculate the LSPR band shift as a function of temperature for each mechanism. The results of the calculations can be seen in Fig. 10. As seen from Fig. 10, the contribution from the thermal expansion of AuNPs is the dominant mechanism. The contribution from electron-phonon scattering is small compared to the contribution from the thermal expansion. This agrees with the results of the modeling performed by Yeshchenko et al. [7] where the volume thermal expansion of the AuNPs was found to have the most effect on the LSPR band shift with changing temperature. The total contribution curve and the fit data for the Ar experiment are nearly identical revealing the accuracy in the experimental determination of the relationship between the LSPR band shift and temperature. The excellent theoretical fitting based on purely temperature dependence of plasmonic property also provides a further exclusion that no chemical effect could occur for the fully sealed particles.

3.2. Temperature sensing using reflection spectroscopy

In case transmission mode measurement is unmanageable, such as that involving a hot or agitating liquid media or beam path blockage by non-transparent vessel walls, reflection spectroscopy is necessary. To develop and examine this type of sensing capability, we introduced a highly reflective metal layer on the backside of the sample as a mirror to reflect an incident light back to a detector except for the part that is absorbed by the sample. Palladium foil was used as the reflective layer due to its optical, chemical, and thermal stability under the present test condition (up to 350 °C in air or Ar). Fig. 11 shows the results of the reflectance tests in 5% O_2 in Ar for the shallow-embedded AuNP sample. Because of black body emission (thermal radiation) from the Pd mirror, the tests were done from high temperature to low temperature. Otherwise, the black body emission would predominate the pure temperature effect of the AuNPs and cause an overall blue shift in the LSPR peak position with temperature. By starting at high temperatures for the UV–vis extinction spectral measurement, the blue shift effect associated with interference from the black body emission of the Pd mirror is eliminated. As shown in Fig. 11, a consistent red shift can be seen with increasing temperature, indicative of the results of the transmission tests.

The mean value of the LSPR peak position at each temperature was plotted to evaluate the temperature dependence of the AuNPs using reflection mode (Fig. 12). The data from the reflectance tests showed the same linear character seen in the transmittance tests. The slope of this linear fit has a value ($0.01103 \pm 2.23 \times 10^{-4}$ nm/°C) similar to the value of the slopes found for the transmittance tests presented above. The similarities in the values of the slopes for the two tests show the reliability of the reflectance tests as a mean of measuring the temperature dependence of the AuNPs. It also further proves the feasibility of the sealed AuNPs to act as a temperature sensor since similar values were achieved even when the AuNP samples were placed in three different environments: air, Ar, and 5% O_2 in Ar. The difference between the slope values of the transmittance and reflectance tests is likely a result of the mechanisms involved in both measurements.

In a transmission measurement, light passing through the sample will take three distinct paths if surface scattering effects are neglected: 1) absorption of light by the AuNPs, 2) reflection by the sample, and 3) transmission of light through the sample. In this case, the light lost by the sample can stem from both absorption of light and reflection by the sample and the output measurements will not accurately reflect how much light was absorbed by the NPs themselves. By relying on the reflection of light back to the detector, light can only do two things if scattering effects are once again neglected: 1) absorption of light by the AuNPs and 2) reflection of light by the sample. This is because of the addition of the Pd mirror, making transmittance of light through the sample effectively zero. Thus, when the reflected light is collected, absorption of light into the AuNPs is the only way light is lost. An extrinsic effect in this case is that the black body emission of metal reflective

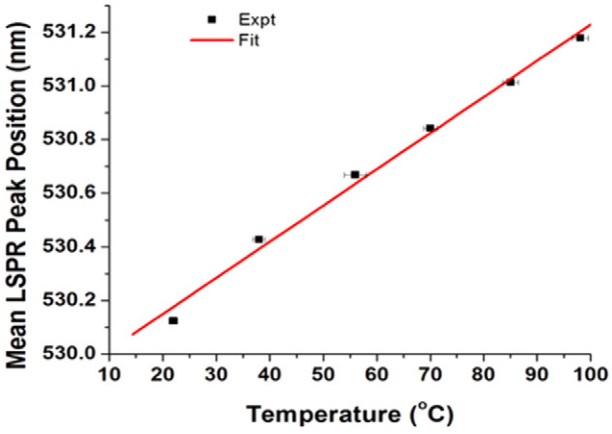

Fig. 14. Results of the reflectance tests in water with (a) the plot of the mean LSPR peak position as a function temperature and (b) the linear fit data.

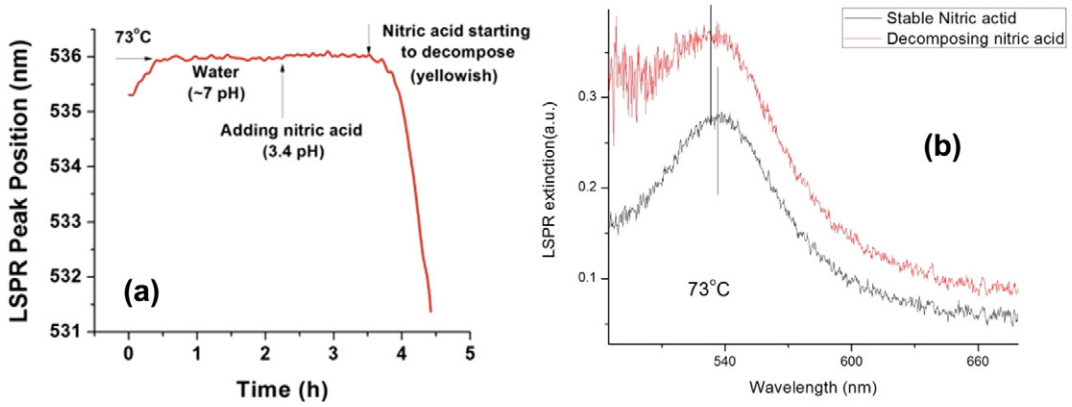

Fig. 15. a) Plot of LSPR peak position vs. time for reflectance tests done in water where the pH of the aqueous environment is changed from neutral to acidic and b) absorbance spectra of nitric acid at constant temperature before and after decomposition showing a noticeable blue shift that is reflected in a).

foils could be captured if the temperature is high, causing an interference effect that may not be able to be completely eliminated.

An advantage of using reflection spectroscopy as opposed to transmission spectroscopy has to do with the versatility of reflection measurements. Unlike the transmittance measurements, the reflection measurements can be realized by relying on a single optical fiber to both direct light beam and collect the reflected light. This allows for a wider range of applications in that an optical fiber based temperature probe can be integrated and provides a much simple and convenient temperature sensing as compared to the transmission set-up. Reflection measurements can be placed in environments where transmission would be difficult or where too much interference would be present in the light's path to achieve accurate and fast results.

3.3. Temperature sensing in aqueous environments

To demonstrate the application versatility, reflectance tests using an optical fiber setup (Fig. 4) were done in water. Fig. 13a shows the response of the deep-embedded sample when it is submerged in water. There is still a clear red shift and peak broadening of the plasmonic peak when the temperature of the water bath is changed from 25 °C to 99 °C. Furthermore, the LSPR peak position of the AuNPs consistently red shifts at each increasing temperature step as evidenced in Fig. 13b. The slight down drift observed at the temperature steps is due to thermal equilibrium in the large water bath after the thermal ramp. The similarity in the behavior of the plasmonic peak even when the AuNPs are submerged in an aqueous environment bodes well for its versatility as a temperature sensor and further emphasizes that the sample remains unaffected by chemical effects. Fig. 14 shows the plot of the mean LSPR peak position at each temperature step as a function of temperature. Examination of the linear fit and the linear fit data (Fig. 14) (a slope of $0.01381 \pm 8.96 \times 10^{-4}$ nm/°C) reveals that the change in LSPR as a function of temperature for the experiments in water follows the same linear trend as the AuNPs did in air. The slope value of the linear fit is close in value to the slope values of the other experiments. Deviations in linearity are likely because the temperature values recorded may not be indicative of the actual temperature of the sample due to the air side cooling across the window and water temperature equilibrium. However, the good linear character in the slope further emphasizes the isolation of the AuNPs from chemical effects and its ability to be used as a pure temperature sensor in various environments. The results of these tests in water also underscore the versatility of measuring the absorbance of the AuNPs using optical probes and reflection measurements.

The pH of the water bath was changed by adding nitric acid to a pH of 3.4 and kept at a constant temperature of 73 °C. As seen from Fig. 15, the addition of acid did not lead to a significant shift the LSPR peak position of the AuNPs. The lack of change in the plasmonic peak of the AuNPs even after changing the chemical environment in the water further emphasizes the complete encapsulation of the AuNPs in the glass substrate. Additionally, the immunity to changing pH environments and the sensor's ability to operate under acidic conditions proves the robustness of the sensor and its ability to withstand harsh conditions.

4. Conclusions

The feasibility of a plasmonic-based temperature sensing was determined for AuNPs fully embedded in a glass matrix. Three different sets of experiments were done to show the relation of the plasmon peak position and temperature: transmission of light through air and Ar environments, reflection of light through 5% O_2 in Ar environments, and reflection of light in water. The change in peak position with temperature for both transmission and reflection experiments in different ambient showed the linear character outlined in the theory. The transmission mode measurements were performed in multiple gas environments to prove the isolation of the temperature effect on the AuNPs from any chemical interference. This proves that the method of embedding the AuNPs into a glass matrix will allow for the development plasmonic temperature sensors. The measurements performed in water showed a similar linear relationship between the plasmonic peak position and temperature as the experiments done in air, proving the versatility of the sensor for different environments.

Conflict of interest

We have no conflict of interest to declare.

Acknowledgements

The authors gratefully acknowledge funding from Bechtel Marine Propulsion Corporation for completion of this work.

References

[1] K.M. Mayer, J.H. Hafner, Localized surface plasmon resonance sensors, Chem. Rev. 111 (2011) 3828–3857.
[2] T.-J. Lin, K.-T. Huang, C.-Y. Liu, Determination of organophosphorous pesticides by a novel biosensors based on localized surface plasmon resonance, Biosens. Bioelectron. 22 (2006) 513–518.
[3] B. Sepúlveda, P.C. Angelomé, L.M. Lechuga, L.M. Liz-Marzán, LSPR-based nanobiosensors, Nano Today 4 (2009) 244–251.
[4] K. Saha, S.S. Agasti, C. Kim, X. Li, V.M. Rotello, Gold nanoparticles in chemical and biological sensing, Chem. Rev. 112 (2012) 2739–2779.
[5] Y. Shao, S. Xu, Y. Wang, W. Xu, Optical fiber LSPR biosensor prepared by gold nanoparticle assembly on polyelectrolyte multilayer, Sensors 10 (2010) 3585–3596.
[6] P.R. Ohodnicki, M.P. Buric, T.D. Brown, C. Matranga, C. Wang, J. Baltrus, M. Andio, Plasmonic nanocomposite thin film enabled fiber optic sensors for simultaneous

gas and temperature sensing at extreme temperatures, Nanoscale 5 (2013) 9030–9039.
[7] O.A. Yeshchenko, I.S. Bondarchuk, V.S. Gurin, I.M. Dmitruk, A.V. Kotko, Temperature dependence of the surface plasmon resonance in gold nanoparticles, Surf. Sci. 608 (2013) 275–281.
[8] U. Kreibig, M. Vollmer, Optical Properties of Metal Clusters, Springer, Berlin, 1995.
[9] G. Sirinakis, R. Siddique, I. Manning, P.H. Rogers, M.A. Carpenter, Development and characterization of Au—YSZ surface plasmon resonance based sensing materials: high temperature detection of CO, J. Phys. Chem. B 110 (2006) 13508–13511.
[10] S. Agnihotri, S. Mukherji, S. Mukherji, Size-controlled silver nanoparticles synthesized over the range 5–100 nm using the same protocol and their antibacterial efficiency, RSC Adv. 4 (2014) 3974–3983.
[11] P.H. Rogers, G. Sirinakis, M.A. Carpenter, Direct observations of electrochemical reactions within Au-YSZ thin films via absorption shifts in the Au nanoparticle surface plasmon resonance, J. Phys. Chem. C 112 (2008) 6749–6757.
[12] P.H. Rogers, M.A. Carpenter, Particle size sensitivity dependence of nanocomposites for plasmonic-based all-optical sensing applications, J. Phys. Chem. C 114 (2010) 11033–11039.
[13] http://www.engineersedge.com/heat_transfer/thermal-conductivity-gases.htm.
[14] A. Dutta, T.P. Sinha, P. Jena, S. Adak, Ac conductivity and dielectric relaxation in ionically conducting soda–lime–silicate glasses, J. Non-Cryst. Solids 354 (2008) 3952–3957.
[15] K. Ujihara, Reflectivity of metals at high temperatures, J. Appl. Phys. 43 (1972) 2376.
[16] V. Synecek, H. Chessin, M. Simerska, The temperature dependence of lattice vibrations in gold from X-ray diffraction measurements, Acta Cryst A26 (1970) 108–113.
[17] N.W. Ashcroft, N.D. Mermin, Solid State Physics, Saunders College, Philadelphia, 1976.